Electron-impact study of S_3 using the *R*-matrix method

Savinder Kaur,* Anand Bharadvaja,† and K. L. Baluja‡
Department of Physics and Astrophysics, University of Delhi, Delhi-110007, India
(Received 24 November 2010; published 17 June 2011)

We have carried out a comprehensive study of electron impact on the open-chain S_3 isomer by using the *R*-matrix method. Elastic (integrated and differential), momentum-transfer, excitation, and ionization cross sections, along with effective collision frequency over a wide electron temperature range (500–30 000 K) have been presented. The target states are represented by including correlations via a configuration interaction technique. The results of the static-exchange, correlated 1-state, and 24-state close-coupling approximations are presented. Our study has detected a shape resonance, six core-excited shape resonances, and one Feshbach resonance in the 24-state model. We detect a stable bound state of S_3^- of $^2B_1$ symmetry having a configuration $\ldots 11a_1^2, \ldots 3b_1^2 4b_1, \ldots 8b_2^2, \ldots 2a_2^2$, with a vertical electronic affinity value of 2.15 eV, and a ionization potential value of 9.77 eV, which are in good agreement with the experimental values of 2.093 ± 0.025 and 9.68 ± 0.03 eV, respectively. The ionization cross sections are calculated using the binary-encounter-Bethe model in which Hartree-Fock molecular orbitals at a self-consistent level are used to calculate kinetic and binding energies of the occupied molecular orbitals. We have used partial waves up to $l = 4$ to represent continuum electron in our *R*-matrix method. A Born top-up procedure is invoked to account for the contribution of partial waves higher than $l = 4$ to obtain converged cross sections.

DOI: 10.1103/PhysRevA.83.062707 PACS number(s): 34.80.Bm, 34.80.Gs, 34.80.Ht

I. INTRODUCTION

Sulfur has drawn considerable interest for several reasons. It has the largest number of allotropes, with many of them comprising cyclic molecules [1–3]. It exhibits allotropy in the solid, molten, and gaseous phases [4]. It is one of the most cosmically abundant second-row elements observed in a radio band in a variety of galactic sources and circumstellar shells of carbon-rich evolved stars [5–7]. It is an excellent candidate for astronomical detection in comets [8] and the atmosphere of Jupiter's moon Io, where S_2 and SO_2 are readily observed [9]. The thiozone or S_3 molecule is observed in supersonic molecular beams, inert gases, interstellar and astronomical sources, with a gas phase at low- and high-resolution spectroscopy. The study of thiozone is further motivated by their expected presence in ancient sedimentary rocks during photolysis of SO_2 resulting in the formation of S_3 [5–10].

The S_3 molecule is of great interest due to its analogy with the important and valence-isoelectronic O_3 molecule. The S_3 molecule, which is a closed shell, is stable at very high temperatures [11]. The S_3 ground state is a singlet with two valence isomers: the open-chain structure with C_{2v} symmetry and the closed (cyclic) chain structure with D_{3h} symmetry [12–18]. The closed D_{3h} form of S_3 lies 6.7 kcal mol^{-1} above the open-chain form [19]. Lenain *et al.* [20] concluded from the observed Raman spectra that the ground-state geometry corresponds to the bent C_{2v} form, just as in O_3. There is a tendency of the second-row atoms to favor bent structures. This observation was further supported by accurate *ab initio* calculations [4,14,15,21], though some semiempirical theories [16,18], supported the cyclic D_{3h} structure. All single configuration Hartree-Fock (HF) calculations, regardless of the level of the theory, predict the ring to be more stable [4,12,14–16,21–23]. However, when electron correlation is considered, the order of stability is reversed [24]. Jones [13] has performed calculations using density functional calculations with the parameter-free local spin density (LSD) approximation for the exchange correlation energy for the low-lying $^1A_1$, $^3A_2$, $^3B_1$, and $^3B_2$ states of S_3. He has reported the vertical excitation energies for these states at two geometries ($\angle SSS = 114^\circ$ and $R_{SS} = 3.78$ a.u. and $\angle SSS = 120^\circ$ and $R_{SS} = 3.76$ a.u.). The LSD approximation predicts near degeneracy between the two forms.

Raghavachari *et al.* [4] have studied small sulfur clusters (S_2–S_{12}) using *ab initio* molecular orbital techniques. The HF method was used in the determination of the molecular geometries for all clusters. They optimized the geometry using efficient gradient techniques with the 3-21G* basis set [valence double-zeta (DZV) sp plus a set of *d*-type polarization functions on each sulfur atom]. In smaller clusters containing multiple bonds, the calculated bond lengths at the HF level are too small, thus emphasizing the need for electron correlation effects to obtain a more reliable geometry.

Fueno and Buenker [21] have reported the calculations using the multireference double-configuration interaction (MRD-CI) method, for S_3 with bond angle of $\angle SSS = 119^\circ$ and bond length $R_{SS} = 1.914$ Å. The bond angles for the C_{2v} symmetry have no bearing on the relative stabilities of the ring isomers. Suomtamo *et al.* [24] have studied the sulfur clusters S_2-S_5 using the molecular valence method. The geometry was optimized using both minimal (MZ) and polarized double-zeta (DZP) basis sets.

Koch *et al.* [25] computed the adiabatic electron affinity of S_3 and the energies of the three low-lying excited electronic states of the thiozone anion at an optimized geometry of the $X\,^2B_1$ ground state employing coupled-cluster theory with

*Also at SGTB Khalsa College, Department of Physics, University of Delhi; sk_savinder2005@yahoo.co.in
†Also at Bhaskaracharya College of Applied Sciences, University of Delhi, New Delhi-110075; anand_bharadvaja@yahoo.com
‡kl_baluja@yahoo.com

single, double, and partially triple excitations [CCSD(T)], second-order multireference perturbation theory [complete active space with second-order perturbation theory (CASPT2)], and multireference configuration interaction [MRCI and internally contracted MR-configuration interaction (IC-MRCI)] methods using a large atomic natural orbital basis set.

Millefiori and Alparone [26] calculated the structure and the dipole polarizabilities of S_n clusters ($n = 2$–12) using density functional theory within the Becke three-parameter Lee-Yang-Parr (B3LYP) approximation and conventional *ab initio* HF and CCSD(T) methods.

The rotational spectrum of S_3 has been observed [5] and precise geometric structure has been derived with S_3 as a bent chain with $R_{SS} = 1.917 \pm 0.001$ Å and an apex angle 117.36° by means of Fourier-transform microwave spectroscopy. Experimentally, Nimlos and Ellison [27] report an electron affinity of S_3 as 2.093 ± 0.025 eV and from Franck-Condon analysis of photoelectron spectra give an estimate for the S-S bond as 1.90 ± 0.05 Å. Berkowitz and Lifshitz [28] deduced the ionization potentials as 9.68 ± 0.03 eV for S_3.

The electron structure of S_3, as O_3, is a mixture of ionic and diradical valence structures, which imparts a multiconfigurational character to the ground-state wave functions. The HF ground-state configuration of the S_3 molecule in the open-chain structure, i.e., in C_{2v} symmetry, is $\ldots 11a_1^2$, $\ldots 3b_1^2$, $\ldots 8b_2^2$, $\ldots 2a_2^2$ and corresponds to $(X\,^1A_1)$ while the unoccupied orbitals are $4b_1^0$, $12a_1^0$, and $9b_2^0$. The orbital $8b_2$ is occupied and the $4b_1$ orbital is empty in C_{2v} symmetry while this occupancy gets reversed in D_{3h} symmetry. Thus the HF ground-state configuration of the S_3 molecule in the closed-chain structure, i.e., in D_{3h} symmetry is $\ldots 11a_1^2$, $\ldots 4b_1^2$, $\ldots 7b_2^2$, $\ldots 2a_2^2$. The $4b_1$ orbital is an antibonding π^* orbital while $8b_2$ is a nonbonding $n\sigma$ orbital, thus showing that the S-S bond distance is shorter in C_{2v} symmetry than in D_{3h} symmetry [14,29]. There are several theoretical methods to determine structures and properties of small structures such as the *ab initio* approach [30–32], the embedded atom methods (EAMs) [33,34], tight-binding molecular dynamics (TBMD) [35,36], pseudopotential density-functional-theory method, and the Langevin molecular dynamics annealing technique (PDFMD) [1], and the coupled-cluster theory [29].

The structure of S_3 is a computational challenge because the S-S bond length is quite sensitive to the level of theory, the size of the basis set employed, and the participation of the low-lying $3d$ orbitals in bonding. This work uses the *ab initio* *R*-matrix method to study the low-energy electron scattering of the S_3 molecule in the fixed-nuclei approximation. The calculations use the UK molecular *R*-matrix code [37,38]. The *R*-matrix method provides cross sections at a large number of scattering energies efficiently. It includes correlation effects and gives an adequate representation of several excited states of the molecule [39]. Our interest lies in low-energy region ($\leqslant$10 eV), where high-level but few-channel methods such as the *R*-matrix works best. The incoming electron can occupy one of the many unoccupied molecular orbitals or can excite any of the occupied molecular orbitals as it falls into another one. These processes give rise to the phenomenon of resonances forming a negative molecular ion for a finite time before the resonance decays into energetically open channels. Below the threshold of the first vibrational channel, the energy loss is due to rotational excitations, which is very important for polar molecules where the cross section becomes enormous. The binary-encounter-Bethe (BEB) ionization cross sections [40,41] are also computed. The BEB cross sections depend on energy (kinetic, binding), the occupation number of the occupied molecular orbitals of the target, and the energy of the incident electron. The electron scattering calculations are performed at a static-exchange (SE) level and close-coupling approximation, by including 1 and 24 target states, namely, the 1-state (CI-1 state) and 24-state close-coupling approximation.

II. METHOD

A. Theory

The *R*-matrix theory [42,43] is well described and thus we give an outline only. The configuration space of the scattering system in an *R*-matrix approach is divided into an inner and an outer region. Both regions are treated differently in accordance with different interactions in each region. Once the scattering electron leaves the inner region, the other target electrons get confined in the inner region.

In the present work the *R*-matrix boundary radius dividing the two regions was chosen to be $12a_0$ centered at the S_3 center of mass. This sphere encloses the entire charge cloud of the occupied and virtual molecular orbitals included in the calculation. At $12a_0$, the amplitudes of the molecular orbitals are less than $10^{-3}a_0^{-3/2}$. However, the continuum orbitals have finite amplitudes at the boundary. Inside the *R*-matrix sphere, the electron-electron correlation and exchange interactions are strong. Short-range correlation is important to describe the resonances. The behavior of the differential cross sections at small scattering angles is dictated by the dipole interaction (if present) and long-range polarization.

A multicentered configuration interaction (CI) wave-function expansion is used in the inner region. The calculation in the inner region is similar to a bound-state calculation, which involves the solution of an eigenvalue problem for $(N + 1)$ electrons in the truncated space, where there are N target electrons and a single scattering electron. Most of the physics of the scattering problem is contained in this $(N + 1)$ electron bound-state molecular structure calculation. Outside the sphere, only long-range multipolar interactions between the scattering electron and the various target states are included. Since only direct potentials are involved in the outer region, a single center approach is used to describe the scattering electron via a set of coupled differential equations. The *R*-matrix is a mathematical entity that connects the two regions. It describes how the scattering electron enters the inner region and how it leaves it. In the outer region, the *R*-matrix on the boundary is propagated outward [44,45] until the inner region solutions can be matched with asymptotic solutions, thus yielding the physical observables such as cross sections. We include only the dipole and quadrupole moments in the outer region.

In the polyatomic implementation of the UK molecular *R*-matrix code [37,38], the continuum molecular orbitals are constructed from atomic Gaussian-type orbitals (GTOs) using basis functions centered on the center of gravity of the molecule. The main advantage of GTOs is that integrals

involving them over all space can be evaluated analytically in closed form. However, a tail contribution is subtracted to yield the required integrals in the truncated space defined by the inner region [37].

The target molecular orbital space is divided into core (inactive), valence (active), and virtual orbitals. The target molecular orbitals are supplemented with a set of continuum orbitals, centered on the center of gravity of the molecule. The continuum basis functions used in polyatomic R-matrix calculations are Gaussian functions and do not require fixed boundary conditions. First, target and continuum molecular orbitals are orthogonalized using Schmidt orthogonalization. Then symmetric or Löwdin orthogonalization is used to orthogonalize the continuum molecular orbitals among themselves and remove linearly dependent functions [37,46]. In general and in this work, all calculations are performed within the fixed-nuclei approximation. This is based on the assumption in which electronic, vibrational, and rotational motions are uncoupled.

In the inner region, the wave function of the scattering system consisting of target plus scattering electron is written using the CI expression

$$\Psi_k^{N+1} = A \sum_i \phi_i^N(x_1, \ldots, x_N) \sum_j \xi_j(x_{N+1}) a_{ijk} + \sum_m \chi_m(x_1, \ldots, x_N, x_{N+1}) b_{mk}, \quad (1)$$

where A is an antisymmetrization operator, x_N is the spatial and spin coordinate of the Nth electron, ϕ_i^N represents the ith state of the N-electron target, ξ_j is a continuum orbital that is spin coupled with the scattering electron, and k refers to a particular R-matrix basis function. Coefficients a_{ijk} and b_{mk} are variational parameters determined as a result of the matrix diagonalization.

The first sum runs over the *24* target states included in the present calculation, which are represented by a CI expansion. It accounts for one electron in a continuum state with the remaining electrons in a target state. To obtain reliable results, it is important to maintain a balance between the N-electron target representation ϕ_i^N and the $(N+1)$ electron scattering wave function. The summation in the second term of Eq. (1) runs over configurations χ_m, where all electrons are placed in target occupied and virtual molecular orbitals. The choice of appropriate χ_m is crucial in this [47]. These are known as L^2 configurations and are needed to account for orthogonality relaxation and for correlation effects arising from virtual excitation to higher electronic state that are excluded in the first expansion. The basis for the continuum electron is parametrically dependent on the R-matrix radius and provides a good approximation to an equivalent basis of orthonormal spherical Bessel functions [48].

We have used $55a_1$, $36b_1$, $36b_2$, and $23a_2$ continuum orbitals. The target and the continuum orbitals of a particular symmetry form an orthonormal set in the inner region, for example, the $12a_1$ orbitals of the target and $55a_1$ orbitals of the continuum are orthonormal to each other. The configuration state functions (CSFs) in the second term in Eq. (1) were constructed by allowing the scattering electron to occupy any of the target occupied or virtual orbitals. This term is responsible for the polarization effects in the 1-state CI calculation also.

B. S_3 target model

There are two isomers of the S_3 molecule: one of C_{2v} symmetry and other of D_{3h} symmetry. The C_{2v} isomer is a prolate asymmetric top closed-chain system having $X\,^1A_1$ as the ground state whereas the D_{3h} isomer has $X\,^1A_1^{'}$ as the ground state. S_3 and O_3 are isovalent homologs. The DZP Gaussian basis set [49] were used, contracted as (12,8,1)/(6,4,1) for S atoms. The diffused functions (with a cutoff exponent 0.1) were avoided as they would extend outside the R-matrix box. The optimized geometry for C_{2v} isomer has $R_{SS} = 1.9037$ Å and $\angle SSS = 117.2506^\circ$, which is close to the optimized geometry having $R_{SS} = 1.912$ Å and $\angle SSS = 117.9^\circ$ for the DZP basis set by Suontamo *et al.* [24] and $R_{SS} = 1.963$ Å and $\angle SSS = 117.4^\circ$ of Ivanic *et al.* [50]. The angle 117.4° is within 2° of that for the isovalent molecule $O_3(116.8^\circ)$, indicating sp^2 hybridization for the apex sulfur. We optimized the ground-state geometry at the HF level using the Gaussian GO3 package. Our main work rests on the C_{2v} isomer but we have carried out a scattering calculation on the D_{3h} isomer in the SE approximation. The optimized geometry for the D_{3h} isomer has a bond length of 2.127 Å with a bonding angle of 60°. The set of occupied and virtual set of orbitals were obtained by the self-consistent field (SCF) calculation for the ground state of the S_3 molecule. This calculation yields occupied orbitals up to $11a_1$, $3b_1$, $8b_2$, and $2a_2$. Their binding energies for the C_{2v} isomer are tabulated in Table I.

TABLE I. S_3 molecular orbital binding and average kinetic energies (in eV) for the DZP basis set at an equilibrium geometry for a C_{2v} isomer.

Molecular orbital	$\lvert B\rvert$	U	N
$1a_1$	2506.65	3296.90	2
$2a_1$	2503.34	3296.82	2
$3a_1$	248.00	509.25	2
$4a_1$	244.85	509.08	2
$5a_1$	184.77	478.92	2
$6a_1$	181.72	477.67	2
$7a_1$	181.60	479.15	2
$8a_1$	32.08	61.99	2
$9a_1$	21.21	72.28	2
$10a_1$	15.35	50.05	2
$11a_1$	10.39	52.77/3	2
$1b_1$	184.80	478.17	2
$2b_1$	181.64	478.16	2
$3b_1$	14.60	42.96	2
$1b_2$	2503.34	3296.82	2
$2b_2$	244.85	509.08	2
$3b_2$	184.84	478.16	2
$4b_2$	181.72	477.67	2
$5b_2$	181.60	479.15	2
$6b_2$	26.98	64.06	2
$7b_2$	15.58	59.85	2
$8b_2$	10.50	50.67/3	2
$1a_2$	181.64	478.16	2
$2a_2$	9.77	45.58/3	2

TABLE II. Dominant configuration, the transition moments (in a.u.), N the number of CSFs, and the vertical excitation energies (in eV) for the target states of S_3 open-chain isomer. The dagger (†) represents the dipole moment.

State C_{2v}	Dominant configuration	Transition moments	N	Vertical Excitation Energy		
				Present $\angle SSS = 117.2506^\circ$ $R_{SS} = 1.9037$ Å	Jones[a] $\angle SSS = 114^\circ$ $R_{SS} = 3.78$ a.u.	Jones[a] $\angle SSS = 120^\circ$ $R_{SS} = 3.76$ a.u.
$X\,^1A_1$	$\ldots 11a_1^2, \ldots 3b_1^2, \ldots 8b_2^2, \ldots 2a_2^2$	0.2791†	4067	0.000	0.0	
$a\,^3B_2$	$(\ldots)2a_2^{-1}4b_1$	–	5802	1.467	1.4	
$b\,^3B_1$	$(\ldots)11a_1^{-1}4b_1$	–	5826	1.510	1.3	
$c\,^3A_2$	$(\ldots)8b_2^{-1}4b_1$	–	5811	1.681	1.2	
$1\,^1A_2$	$(\ldots)8b_2^{-1}4b_1$	–	3843	1.811	1.5	1.71
$1\,^1B_1$	$(\ldots)11a_1^{-1}4b_1$	0.0489	3858	1.861	1.6	1.52
$d\,^3B_2$		–	5802	3.447		
$2\,^1A_1$	$(\ldots)11a_1^{-1}12a_1$	0.0062	4067	3.643		
$1\,^1B_2$	$(\ldots)2a_2^{-1}4b_1$	1.0638	3962	3.714	2.3	1.97
$e\,^3A_2$		–	5811	4.503		
$f\,^3B_1$		–	5826	4.676		
$2\,^1A_2$		–	3843	4.871		
$3\,^1A_1$		0.0972	4067	5.073		
$2\,^1B_1$		0.114	3858	5.089		
$g\,^3A_1$		–	5727	5.142		
$h\,^3A_1$		–	5727	5.243		
$i\,^3B_2$		–	5802	5.250		
$2\,^1B_2$		0.0616	3962	5.401		
$j\,^3A_2$		–	5811	5.708		
$k\,^3B_1$		–	5826	5.969		
$3\,^1A_2$		–	3843	6.065		
$3\,^1B_1$		0.0192	3858	6.298		
$3\,^1B_2$		0.5702	3962	6.326		
$l\,^3A_1$		–	5727	6.977		

[a]Reference [13].

By Koopmans' theorem, the first ionization energy is 9.77 eV, which is in agreement with the experimental value of 9.68 ± 0.03 eV [28]. The SCF calculations do not provide a good representation of the target states. The CI calculations were performed, which resulted in the lowering of the ground state and excited states. Also, the correlation introduced provides a better description of the target wave function and excitation energies. The SCF ground-state energy for the S_3 molecule is -1192.4538 a.u., in comparison to the HF value of $-1192.472\,55$ a.u. of Raghavachari *et al.* [4], while our CI ground-state energy gets lowered to -1192.5379 a.u., which compares well with other works in literature [4,25,26,50]. The HF value refers to an extremely large basis set function as compared to a SCF calculation.

In the CI model, 30 frozen electrons were distributed in the $1a_1^2 2a_1^2 \ldots 7a_1^2$, $1b_1^2 2b_1^2$, $1b_2^2 2b_2^2 \ldots 5b_2^2$, $1a_2^2$ configuration and the remaining 18 electrons are allowed to move freely in nine molecular orbitals $8a_1 \ldots 11a_1$, $3b_1$, $6b_2 \ldots 8b_2$, $2a_2$. In our model we allow single as well as double excitations from the HF occupied orbitals to any one of the available virtual orbitals. There are also some selected triple excitations included, for example $11a_1 \rightarrow 12a_1$, $3b_1 \rightarrow 4b_1$, and $8b_2 \rightarrow 9b_2$. The vertical eletronic affinity (VEA) was computed using bound state calculations by including the continuum electron basis functions centered at the origin. The stable bound state of S_3^- was detected having a VEA value of 2.1514 eV, in good agreement with 2.093 ± 0.025 eV experimental value [27]. The dipole moment is 0.279 013 a.u. or 0.7086 D, which is close to the value of 0.56 D of Millefiori *et al.* [26], while the components of the quadrupole moments Q_{20} and Q_{22} are 0.631 23 and 2.328 82 a.u., respectively. The correlational energy of the anion with an additional weakly bound electron is much higher than that of the neutral species. A good description of the extra electron requires one-particle basis set augmented by a diffuse function as well as functions of high angular momentum.

In Table II, we list the dominant configuration, the transition moments N, the number of CSFs and the vertical excitation energies for the target states. The excited states are formed by the excitation of an electron from the occupied a_1, b_1, b_2, and a_2 orbitals to the vacant orbitals. Our vertical transition energies for the target states are in good accord with the density functional calculations of Jones [13]. The differences arise due to the different geometry, basis set, the active space, and the correlation effects used in our calculation. This is due to the restriction imposed by R-matrix method of using only a single basis set to represent all the target states. In the R-matrix approach it is computationally convenient to use the same set of basis functions for all the target states. This is also a source of certain discrepancies in the target thresholds

In the 1-state CI model we include only the ground state, which is correlated. With the present DZP basis function

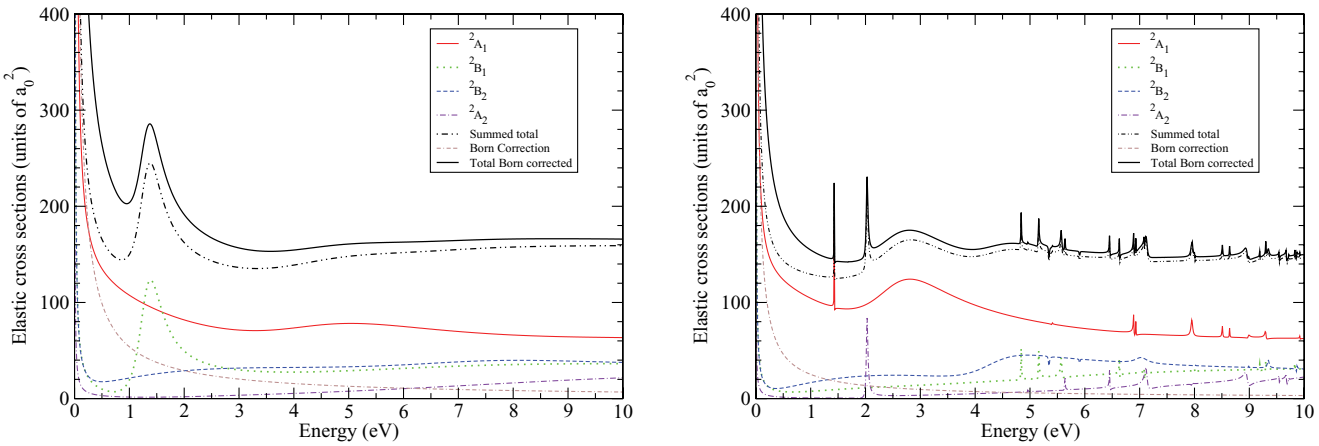

FIG. 1. (Color online) Elastic cross sections of the electron impact on the S_3 molecule. Thin solid curve, $^2A_1$; dotted curve, $^2B_1$; dashed curve, $^2B_2$; dashed-dotted curve, $^2A_2$; single-dashed-double-dotted curve, total summed; double-dashed-dotted-curve, Born correction; thick solid line, total Born corrected. (a) Static exchange. (b) CI-1 state.

we find that the ground state of the C_{2v} isomer is lower by 9.84 kcal/mol with respect to the ground state of the D_{3h} isomer at their corresponding optimized geometry in CI-1 state model. This value is slightly higher than the value 9.2 kcal/mol of Koch *et al.* [25], who used the complete active space self-consistent field approximation (CASSCF) and 8.5 kcal/mol of Millefiori *et al.* [26], which use more elaborate correlation effects.

C. Scattering model

We have included 24 target states, taking three each in the singlet, $^1A_1$,$^1B_1$,$^1B_2$,$^1A_2$, and triplet, $^3A_1$, $^3B_1$, $^3B_2$, $^3A_2$, symmetries in the trial wave function describing the electron plus target system. Calculations were performed for doublet scattering states with A_1, A_2, B_1, and B_2 symmetries. Continuum orbitals up to g partial wave ($l = 4$) were represented by Gaussians centered at the molecule center of gravity [48].

Due to the presence of the long-range dipole interaction, the elastic cross sections are formally divergent in the fixed-nuclei approximation as the differential cross section is singular in the forward direction. To obtain converged cross sections, the effect of rotation must be included, along with a very large number of partial waves.

The effects of partial waves with $l > 4$ were included using a Born correction via a closure approach [51,52]. This correction is applied at the cross-section level at all energies. Our partial g-wave cross section using the R-matrix method nearly coincided with the g-wave and Born results in the entire scattering energy region. This establishes the correctness of our procedure to use the Born correction beyond the g-partial wave.

The maximum number of coupled channels in our scattering calculation is 150. The number of CSFs for a typical doublet scattering symmetry is ∼80 000. Due to the small dipole moment (0.2790 a.u. or 0.7086 D) of the ground state, we have propagated the R-matrix to a radius of $50a_0$. The propagated solutions at $50a_0$ are matched with the asymptotic boundary conditions yielding K matrices from which we can extract integral cross sections using standard formulas.

III. RESULTS

A. Elastic and inelastic total cross sections

In Figs. 1(a) and 1(b) we present the elastic cross sections of electron impact on the S_3 molecule in the SE model and the CI-1 state model, respectively. We have shown the contribution of each symmetry. In the SE calculation, exchange is included and the target molecule is not allowed to be perturbed and hence polarization is assumed to be minimum or zero. In the CI-1 state, exchange is included and the target molecule is allowed to be perturbed and hence polarization is included. Our SCF calculation indicates that the first virtual molecular orbital $4b_1$ has energy of −1.68 eV. The scattering electron occupies this molecular orbital and gives rise to a shape resonance in $^2B_1$ symmetry at ∼1.5 eV as shown in Fig. 1. This resonance is due to lack of correlated effects in the SE approximation. When correlation effects are included via CI in the ground state, this resonance is expected to become a bound state. This we show in Fig. 1(b) in the CI-1 state model. Here, the shape resonance in $^2B_1$ symmetry, which was detected in the SE model, vanishes and becomes a bound state. We instead now have a shape resonance in $^2A_1$ symmetry at ∼3 eV with an electron configuration $(X\,^1A_1)12a_1$. We also see a sharp resonance in the $^2A_2$ symmetry at ∼2 eV and a broad resonance in the $^2B_2$ symmetry at ∼4.7 eV. The other small peaks that we see could be due to pseudoresonances. These peaks get wiped out when more correlation is included in the 24-state model, as can be seen in Fig. 2. Due to the presence of an angular barrier for symmetries other than A_1, the elastic cross sections are expected to start from zero at low energies. Our results for these symmetries are not accurate for energies below 0.5 eV. This is the inherent numerical problem in the R-matrix method in which uncontracted continuum wave functions are used.

When more correlation is added as in our 24-state model, which include more polarization generated by inclusion of excited states, we see that in Fig. 2, the shape resonance in $^2A_1$ is shifted to a lower energy at ∼1.66 eV. This has configuration $X\,^1A_1(12a_1)$ and a width of 0.91 eV. The corresponding resonances in the $^2A_2$ and $^2B_2$ symmetry shift to 0.84 and 3.45 eV, respectively. The resonance in $^2A_2$ is very sharp while

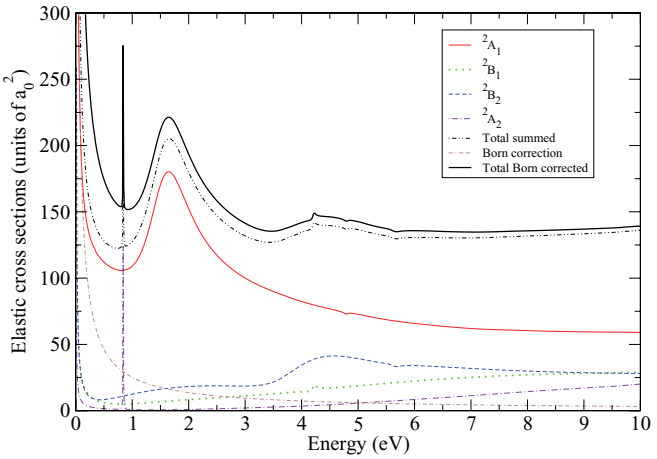

FIG. 2. (Color online) 24-state R-matrix elastic cross sections of the electron impact on the S_3 molecule. Thin solid curve, $^2A_1$; dotted curve, $^2B_1$; dashed curve, $^2B_2$; dashed-dotted curve, $^2A_2$; single-dashed-double-dotted curve, total summed; double-dashed-dotted-curve, Born correction; thick solid line, total Born corrected.

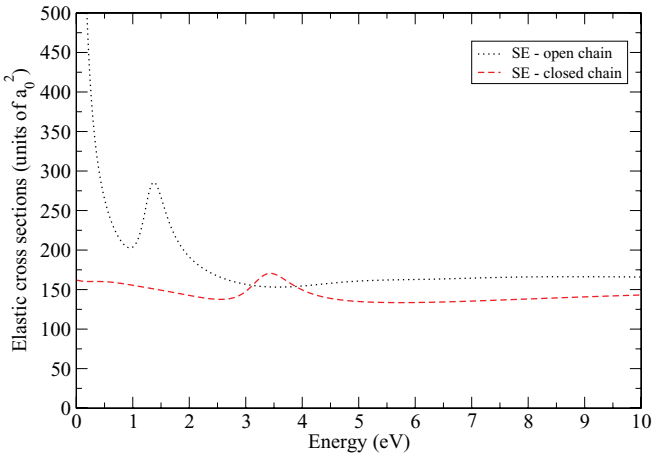

FIG. 3. (Color online) Elastic cross sections of the electron impact on the S_3 molecule in the SE model. Dotted curve, open-chain isomer (C_{2v}); dashed-dotted curve, closed-chain isomer (D_{3h}).

in $^2B_2$ it is broad with a width of 1.16 eV. Further, $^2A_2$ with a configuration ($2a_2^{-1}4b_1^2$) decays to a^3B_2 parent state, which is higher and thus is a Feshbach resonance. The resonance with configuration $^2B_2 : 8b_2^{-1}4b_1^2$ decays to its parent state $1\,^1A_2$ and thus is a core-excited shape resonance.

In Fig. 3 we have compared the elastic cross sections for the two isomers in the SE model. The cross sections for the D_{3h} symmetry are lower than the corresponding C_{2v} cross section because the dipole moment of the D_{3h} isomer is almost zero, having a value of 0.1025×10^7 a.u. The frontier SCF orbitals of the D_{3h} isomer are rearranged as compared to the C_{2v} case. The lowest unoccupied molecular orbital (LUMO) of C_{2v} is $4b_1$, with an orbital energy of -1.68 eV, whereas for D_{3h} the LUMO ($8b_2$) energy is 0.79 eV. The shape resonance in the C_{2v} case in the SE model becomes a bound state in the D_{3h} case at the same level of approximation, indicating an absence of this resonance. However, we see a resonance at 3.45 eV due to the $^2B_2$ symmetry in the D_{3h} case.

In Figs. 4–7 we have shown the inelastic cross sections from the ground state $X\,^1A_1$ to the first five states $a\,^3B_2$, $b\,^3B_1$, $c\,^3A_2$, $1\,^1A_2$, and $1\,^1B_1$, whose vertical excitation thresholds along with their dominant configuration and the number of CSFs included in the CI expansion are given in Table II.

The two transitions in Figs. 4(a) and 4(b) are spin-forbidden transitions. Figure 4(a) depicts $X\,^1A_1 \rightarrow a\,^3B_2$ excitation cross section in which we also show the individual contributions of each scattering symmetry. We notice some interesting features here. The maximum contribution is of $^2B_2$ scattering symmetry. In $^2B_2$ there are peaks at 3.45 and 5.79 eV. The widths of these peaks are 1.16 and 0.26 eV, respectively. The peak at 3.45 eV is the signature of the core-excited shape resonance as also detected in the elastic cross sections in Fig. 2. The peak at 5.79 eV is also a core-excited shape with configuration $^2B_2 : 8b_2^{-1}4b_1^2$, with $j\,^3A_2$ as the parent state. In $^2B_1$ there is a peak at $\sim$4.2 eV with a width of 0.05 eV. It is a core-excited shape resonance with a configuration of $(11a_1^{-1}4b_1 12a_1)^2B_1$ and decays to the parent state $1\,^1B_1$ after the $12a_1$ molecular orbital is detached.

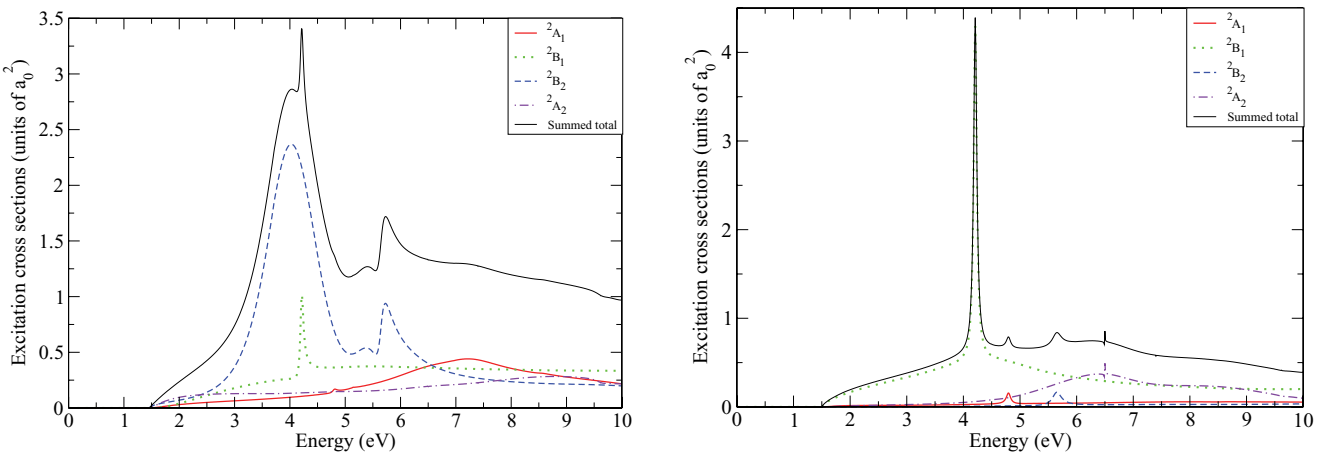

FIG. 4. (Color online) Electron impact excitation cross sections from the ground $X\,^1A_1$ state of the S_3 molecule to the (a) $a\,^3B_2$ state (b) $b\,^3B_1$ state in 24-state model. Thin solid curve, $^2A_1$; dotted curve, $^2B_1$; dashed curve, $^2B_2$; dashed-dotted curve, $^2A_2$; thick solid line, total summed.

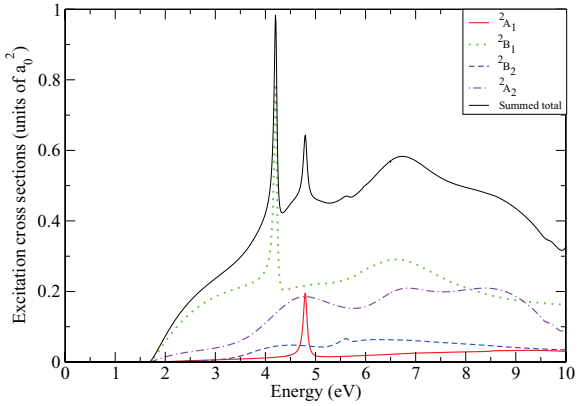

FIG. 5. (Color online) Electron-impact excitation cross sections from the ground $X\,^1A_1$ state of the S_3 molecule to the $c\,^3A_2$ state. Thin solid curve, $^2A_1$; dotted curve, $^2B_1$; dashed curve, $^2B_2$; dashed-dotted curve, $^2A_2$; thick solid line, total summed.

Figure 4(b) depicts a $X\,^1A_1 \rightarrow b\,^3B_1$ excitation cross section. The maximum contribution is that of $^2B_1$ symmetry. In $^2B_1$ there is a peak at ~4.2 eV, as discussed in Fig. 4(a). The peak at ~6.5 eV in $^2A_2$ symmetry is a broad resonance. The peak in $^2A_1$ at 4.75 eV with a configuration of $(11a_1^{-1}3b_1^2)^2A_2$ has a width of 0.17 eV, and is a core-excited shape resonance which decays to the parent state $f\,^3B_1$.

Figure 5 depicts a $X\,^1A_1 \rightarrow c\,^3A_2$ excitation cross section in which we also show the individual contributions of each scattering symmetry. The contributions of the $^2B_1$ and $^2A_2$ symmetries are larger than the other two symmetries. We see a peak in the $^2B_1$ symmetry at 4.2 eV. This was as seen earlier in Figs. 4(a) and 4(b). There is a resonance in $^2A_2$ with a configuration $(2a_2^{-1}4b_1^2)^2A_2$ at 4.67 eV of width 0.62 eV. It is a core-excited shape resonance with a parent state $1\,^1B_2$.

Figure 6 depicts a $X\,^1A_1 \rightarrow 1\,^1A_2$ excitation cross section. This transition is symmetry forbidden. The cross section of $^2B_1$ symmetry attains a peak value at ~4.2 eV while those of $^2B_2$ and $^2A_1$ attain a peak value at 5.79 and 4.75 eV, respectively.

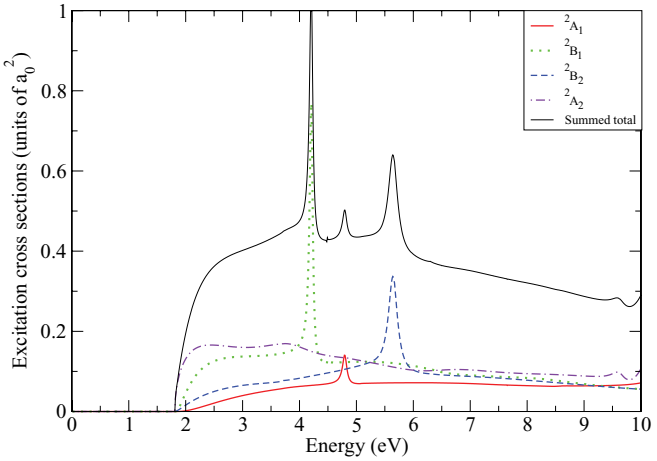

FIG. 6. (Color online) Electron-impact excitation cross sections from the ground $X\,^1A_1$ state of the S_3 molecule to the $1\,^1A_2$ state. Thin solid curve, $^2A_1$; dotted curve, $^2B_1$; dashed curve, $^2B_2$; dashed-dotted curve,$^2A_2$; thick solid line, total summed.

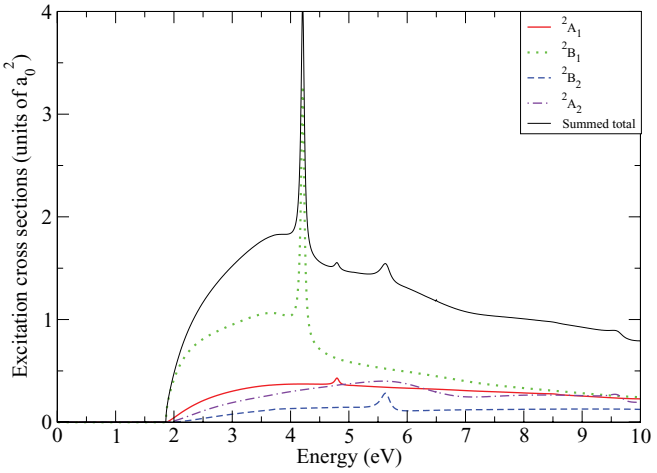

FIG. 7. (Color online) Electron-impact excitation cross sections from the ground $X\,^1A_1$ state of the S_3 molecule to the $1\,^1B_1$ state. Thin solid curve, $^2A_1$; dotted curve, $^2B_1$; dashed curve, $^2B_2$; dashed-dotted curve, $^2A_2$; thick solid line, total summed; double-dashed-dotted-curve, Born correction; thick solid line, total Born corrected.

These resonances have been discussed while describing Figs. 4 and 5.

In Fig. 7, we have shown excitation cross sections for the transition $X\,^1A_1 \rightarrow 1\,^1B_1$. This is the first transition that is dipole allowed. Peaks in $^2B_1$, $^2A_1$, and $^2B_2$ have been discussed in earlier figures.

The resonance position E_r and the resonance width Γ_r parameters of the resonances yielded by 24-state close-coupling calculations are given in Table III. These parameters were obtained by fitting eigenphase sums to the Breit-Wigner profile [53].

B. Ionization cross section

The BEB cross section is rather sensitive to the ionization energy used in the calculation. The ionization energy in our calculation is 9.77 eV, which is deduced from Koopmanns' theorem and is in good agreement with the experimental values of 9.68 ± 0.03 eV [28]. The molecular orbital data used in calculation of BEB cross section is given in Table I. These molecular orbitals used in our CI model were obtained through a SCF calculation, so only this set of molecular orbitals is used to calculate the BEB cross sections. The ionization cross

TABLE III. Resonance parameters of S_3.

Electronic configuration of resonant state	E_r (eV)	Γ_r (eV)	Type of resonance	Parent state
$^2A_1 : X\,^1A_1(12a_1)$	1.66	0.91	Shape	$X\,^1A_1$
$^2A_1 : (\ldots)11a_1^{-1}3b_1^2$	4.75	0.17	Core excited	$f\,^3B_1$
$^2B_2 : (\ldots)8b_2^{-1}4b_1^2$	3.45	1.16	Core excited	$1\,^1A_2$
$^2B_2 : (\ldots)8b_2^{-1}4b_1^2$	5.79	0.26	Core excited	$j\,^3A_2$
$^2B_1 : (\ldots)11a_1^{-1}4b_1 2a_1$	4.20	0.05	Core excited	$1\,^1B_1$
$^2A_2 : (\ldots)2a_2^{-1}4b_1^2$	0.84	0.01	Feshbach	$a\,^3B_2$
$^2A_2 : (\ldots)2a_2^{-1}4b_1^2$	6.50	0.02	Core excited	$3\,^1B_2$
$^2A_2 : (\ldots)2a_2^{-1}4b_1^2$	4.67	0.625	Core excited	$1\,^1B_2$

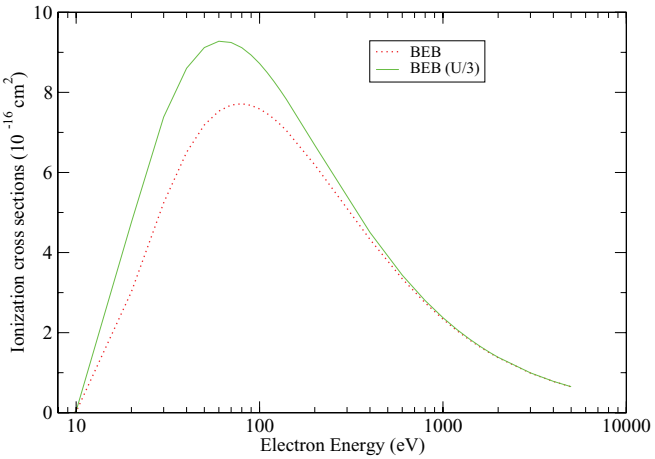

FIG. 8. (Color online) Electron-impact BEB ionization cross sections of the S_3 molecule. Dotted curve, BEB; solid curve, modified BEB

section σ is obtained by summing over each orbital cross section σ_i, where

$$\sigma_i(t) = \frac{S}{t+u+1}\left\{\frac{1}{2}\left(1-\frac{1}{t^2}\right)\ln t + \left[\left(1-\frac{1}{t}\right)-\frac{\ln t}{t+1}\right]\right\}, \tag{2}$$

where $t = T/B$, $u = U/B$, and $S = 4\pi a_0^2 N(R/B)^2$. Here, R is the Rydberg energy, T is the kinetic energy of the incident electron, U is the orbital kinetic energy, N is the electron occupation number, and B is the binding energy of the orbital.

We have calculated electron-impact ionization cross sections of S_3 by using the standard formalism of the BEB model [40,41]. This formalism requires the binding energy and kinetic energy of each occupied molecular orbital in a molecular structure calculation. The parameter Q of the BEB formalism is set to unity. The BEB cross sections are given in Fig. 8 from threshold (9.77 eV) to 5000 eV. The cross section rises from threshold to a peak value of 7.71 Å^2 at 80.0 eV and then shows $\ln E/E$ behavior as E approaches higher values.

According to the Mulliken population analysis, the molecular orbitals $11a_1$, $8b_2$, and $2a_2$ comprise more than a 90% contribution from the $3p$ atomic orbital of sulfur. We have therefore divided the kinetic energy of these molecular orbitals by the principal quantum number $n = 3$. The modified BEB ionization cross sections [54] are larger than the unmodified BEB ionization cross sections. However, the peak now occurs at a 60 eV impact energy with a value of 9.87 Å^2. We note that earlier we have observed peaks in the BEB cross sections for SOS molecule [55] also at 80 and 60 eV for BEB and modified BEB ionization cross sections respectively.

C. Differential cross section

The evaluation of the differential cross sections (DCSs) provides a more stringent test for any theoretical model. The DCS for a general polyatomic molecule is given by the familiar expression

$$\frac{d\sigma}{d\Omega} = \sum_L A_L P_L(\cos\theta), \tag{3}$$

where P_L is a Legendre function. The A_L coefficients have already been discussed in detail in Gainturco and Jain [56]. For polar molecules this expansion over L converges slowly. We use the closure formula to accelerate the convergence of DCS,

$$\frac{d\sigma}{d\Omega} = \frac{d\sigma^B}{d\Omega} + \sum_L \left(A_L - A_L^B\right) P_L(\cos\theta). \tag{4}$$

The superscript B denotes that the relevant quantity is calculated in the Born approximation with an electron-point dipole interaction. The convergence of the series is now rapid since the contribution from the higher partial waves to the DCS is dominated by the electron-dipole interaction. The quantity

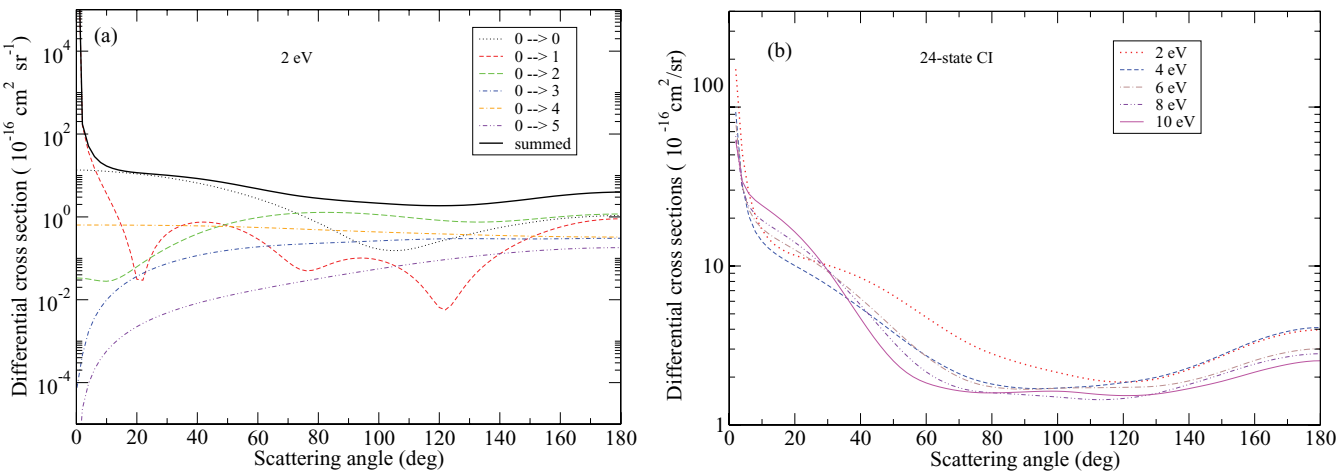

FIG. 9. (Color online) (a) Electron-impact R-matrix rotationally resolved state-to-state ($J \rightarrow J'$) cross sections of S_3 at 2 eV in the 24-state model: Thin dotted curve, $0 \rightarrow 0$; thin dashed curve, $0 \rightarrow 1$; big dashed curve, $0 \rightarrow 2$; dashed-dotted curve, $0 \rightarrow 3$; double-dashed-dotted curve, $0 \rightarrow 4$; double-dotted-dashed curve, $0 \rightarrow 5$; thick curve, summed (over J') results. (b) Electron-impact R-matrix DCS of S_3 differential cross sections in the 24-state model: Dotted curve, 2 eV; dashed curve, 4 eV; dashed-dotted curve, 6 eV; dashed-double-dotted curve, 8 eV; thin solid curve, 10 eV.

$d\sigma^B/d\Omega$ for any initial rotor state $|J\tau\rangle$ is given by the sum over all the final rotor states $|J'\tau'\rangle$,

$$\frac{d\sigma^B}{d\Omega} = \sum_{J'\tau'} \frac{d\sigma^B}{d\Omega}(J\tau \to J'\tau'). \tag{5}$$

The expression for the state-to-state rotationally inelastic DCS, $d\sigma^B/d\Omega(J\tau \to J'\tau')$, for a spherical top, a symmetric top, and an asymmetric top molecule are given by Sanna and Gianturco [57]. We used the calculated rotational constants for S_3, which are $A = 0.804\,577\,206$ cm^{-1}, $B = 0.099\,727\,888\,5$ cm^{-1} and $C = 0.088\,729\,773\,1$ cm^{-1}, which are calculated at the geometry used in the present calculation.

In Fig. 9(a) we show our calculated rotationally resolved DCS for electron scattering by S_3 at an incident energy of 2 eV. The scattering is dominated by the elastic component $0 \to 0$ and the dipole component $0 \to 1$. As J' increases, the cross sections decrease; this shows that, by $J' = 5$, we have obtained almost convergent results. In Fig. 9(b) we show DCSs which are obtained by summing the rotational cross sections for all processes $0 \to (J' = 0\text{–}5)$ at selected energies of 2, 4, 6, 8, and 10 eV. The DCSs at all the energies show a steep rise as the scattering angle approaches zero. This is due to the dipolar nature of the target. Besides this, the data on DCS is further used to calculate the momentum-transfer cross section (MTCS) that shows the weightage of backward-angle scattering. We have calculated DCSs by using the POLYDCS program of Sanna and Gianturco [57] that requires basic molecular input parameters along with K matrices evaluated in the R-matrix scattering calculation.

However, since the DCSs are not very sensitive to correlation effects for backward scattering, we expect our MTCSs to be quite reliable, which are shown in Fig. 10 in the 1–10 eV range. It provides a useful input in solving the Boltzmann equation for the electron distribution function. From Fig. 10, we observe that the MTCS decreases with increasing energy. The peak near 1.5 and 4 eV are due to the effect of resonances. In contrast to the diverging nature of DCS in the forward direction, MTCSs show no singularity due to the weighting factor $(1 - \cos\theta)$, where θ is the scattering angle. This factor vanishes as $\theta \to 0$. The MTCS is useful in the study of electrons drifting through a molecular gas.

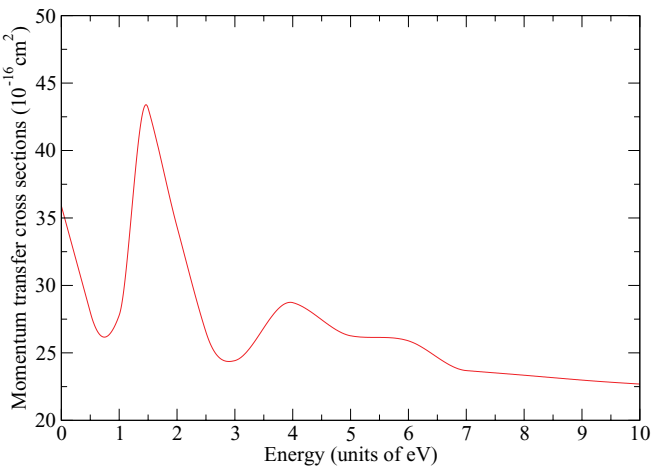

FIG. 10. (Color online) Momentum transfer cross sections of the S_3 molecule ground state, Solid curve, 24-state result.

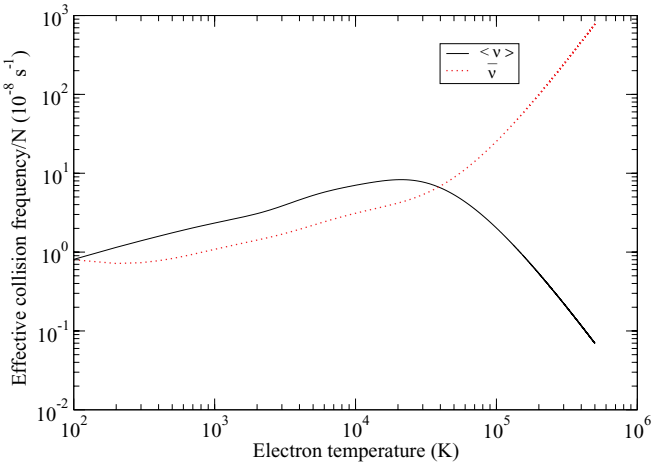

FIG. 11. (Color online) Effective collision frequency of the S_3 molecule ground state. Solid curve, $\langle\nu\rangle$; dotted curve $\bar{\nu}$.

D. Effective collision frequency of electrons

Using the MTCS data, we evaluated two types of the effective electron-S_3 collision frequency $\langle\nu\rangle$ and $\bar{\nu}^{-1}$, from Baille *et al.* [58]. These are given by the following expressions in which it is assumed that the electrons follow a Maxwell-Boltzmann distribution,

$$\langle\nu\rangle = \frac{8}{3\pi^{1/2}} N \left(\frac{m_e}{2kT_e}\right)^{5/2} \int_0^\infty v^5 Q^m(v) e^{-\frac{m_e v^2}{2kT_e}} dv \tag{6}$$

and

$$\bar{\nu}^{-1} = \frac{8}{3\pi^{1/2} N} \left(\frac{m_e}{2kT_e}\right)^{5/2} \int_0^\infty \frac{v^3}{Q^m(v)} e^{-\frac{m_e v^2}{2kT_e}} dv. \tag{7}$$

Here, N is the number density of molecules, m_e is the electron mass, k is the Boltzmann factor, T_e is electron temperature, v is the velocity of the electron, and $Q^m(v)$ is the velocity-dependent MTCS. These are plotted in Fig. 11. These collision frequencies are related to transport properties such as the mean free path, mobilities, and diffusion coefficients. These find applications in the study of electrons swarming through molecular gases.

IV. CONCLUSIONS

We have carried out a detailed study of electron impact on an open-chain S_3 isomer by using the R-matrix method. We have presented results for various types of cross sections. The vertical electronic affinity and the ionization potentials are in good agreement with the experiment. The data generated for MTCS has been fruitfully employed to calculate collision frequencies which are useful for the evaluation of transport coefficients. Our study has detected a shape resonance , a Feshbach resonance, and six core-excited shape resonances in the 24-state model. The ionization cross section presented in the BEB model may be useful to experimentalists as resource data.

[1] B. Yu-Lin, C. Xiang-Rong, Y. Xiang-Dong, and L. Peng-Fei, Acta Phys. Chim. Sin. **12**, 1102 (2003).

[2] J. Donohue, *The Structures of the Elements* (Wiley, New York, 1974), Chap. 9.

[3] R. Steudell, *Studies in Inorganic Chemistry 5*, Vol. 5, edited by A. Muller and B. Krebs (Elsevier, Amsterdam, 1984), p. 13.

[4] K. Raghavachari, C. M. Rohlfing, and J. S. Binkley, J. Chem. Phys. **93**, 5862 (1990).

[5] M. C. McCarthy, S. Thorwirth, C. A. Gottlieb, and P. Thaddeus, J. Am. Chem. Soc. **126**, 4096 (2004).

[6] M. C. McCarthy, S. Thorwirth, C. A. Gottlieb, and P. Thaddeus, J. Chem. Phys. **121**, 632 (2004).

[7] C. A. Gottlieb, S. Thorwirth, M. C. McCarthy, and P. Thaddeus, Astrophys. J. **619**, 939 (2005).

[8] D. Bockelee-Morvan and J. Crovisier, *The Promise of the Herschel Space Observatory*, edited by G. L. Pilbratt, J. Cernicharo, A. M. Heras, T. Prusti, and R. Harris. ESA SP-460 (ESA, Noordwijk, 2001), p. 279.

[9] J. R. Spencer, K. L. Jessup, M. A. McGrath, G. E. Ballester, and Yelle, Science **288**, 1208 (2000).

[10] S. Thorwirth, M. C. McCarthy, C. A. Gottlieb, P. Thaddeus, H. Gupta, and J. F. Stanton, J. Chem. Phys. **123**, 054326 (2005).

[11] N. N. Greenwood and A. Earnshaw, *Chemistry of the Elements* (Pergamon, London, 1984).

[12] N. R. Carlsen and H. F. Schaefer, Chem. Phys. Lett. **48**, 390 (1977).

[13] R. O. Jones, J. Chem. Phys. **84**, 318 (1986).

[14] J. E. Rice, R. D. Amos, N. C. Handy, T. J. Lee, and H. F. Schaefer, J. Chem. Phys. **85**, 963 (1986).

[15] H. Basch, Chem. Phys. Lett. **157**, 129 (1989).

[16] N. C. Baird, J. Mol. Struct. Theochem. **137**, 1 (1986).

[17] D. Hohl, R. O. Jones, R. Carr, and M. Parrinello, J. Chem. Phys. **89**, 6823 (1988).

[18] K. Jug and R. Iffert, J. Mol. Struct. Theochem. **186**, 347 (1989).

[19] Z. Azizi, B. O. Roos, and V. Veryazov, Phys. Chem. Chem. Phys. **8**, 2727 (2006)

[20] P. Lenain, E. Picquenard, J. L. Lesne, and J. Corset, J. Mol. Struct. **142**, 355 (1986).

[21] T. Fueno and R. J. Buenker, Theor. Chim. Acta **73**, 123 (1988).

[22] W. L. Feng and O. Novaro, Int. J. Quantum. Chem. **26**, 521 (1984).

[23] W. L. Feng, O. Novaro, and Garcia-Prieto, Chem. Phys. Lett. **111**, 297 (1984a).

[24] R. J. Suontamo, R. S. Laitinen, and T. A. Pakkanen, J. Mol. Struct., Theochem. **313**, 189 (1994).

[25] W. Kotch, J. Natterer, and C. Heinemann, J. Chem. Phys. **102**, 6159 (1995).

[26] S. Millefiori and A. Alparone, J. Chem. Phys. A **105**, 9489 (2001).

[27] M. R. Nimlos and G. B. Ellision, J. Phys. Chem. **90**, 2574 (1986).

[28] J. Berkowitz and C. Lipshitz, J. Chem. Phys. **48**, 4346 (1968).

[29] J. S. Fransisco, J. R. Lyons, and I. H. Williams, J. Chem. Phys. **123**, 054302 (2005).

[30] O. Cheshnovsky, S. H. Yang, C. L. Pettiette, M. J. Craycraft, Y. Liu, and R. E. Smalley, Chem. Phys. Lett. **138**, 119 (1987).

[31] B. X. Li and P. L. Cao, Phys. Rev. A **62**, 023201 (2000).

[32] Z. Y. Lu, C. Z. Wang, and K. M. Ho, Phys. Rev. B **61**, 2329 (2000).

[33] V. G. Grigoryan and M. Springborg, Phys. Chem. **3**, 5135 (2001).

[34] J. P. K. Doye and D. J. Wales, New J. Chem. **22**, 733 (1998).

[35] J. L. Wang, J. J. Zhao, F. Ding, W. F. Shen, H. Lee, and G. H. Wang, Solid State Commun. **117**, 593 (2001).

[36] J. J. Zhao, J. L. Wang, and G. H. Wang, Phys. Lett. A **275**, 281 (1993).

[37] L. A. Morgan, C. J. Gillan, J. Tennyson, and X. Chen, J. Phys. B **30**, 4087 (1997).

[38] L. A. Morgan, J. Tennyson, and C. J. Gillan, Comput. Phys. Commun. **114**, 120 (1998).

[39] J. Tennyson, J. Phys. B **29**, 1817 (1996).

[40] Y. K. Kim and M. E. Rudd, Phys. Rev. A **50**, 3954 (1994).

[41] W. Hwang, Y. K. Kim, and M. E. Rudd, J. Chem. Phys. **104**, 2956 (1996).

[42] P. G. Burke and K. A. Berrington, *Atomic and Molecular Processes: An R-matrix Approach* (Institute of Physics, Bristol, 1993).

[43] C. J. Gillan, J. Tennyson, and P. G. Burke, *Computational Methods for Electron-Molecule Collisions*, edited by W. M. Huo and F. A. Gianturco (Plenum, New York, 1995).

[44] K. L. Baluja, P. G. Burke, and L. A. Morgan, Comput. Phys. Commun. **27**, 299 (1982).

[45] L. A. Morgan, Comput. Phys. Commun. **31**, 419 (1984).

[46] B. M. Nestmann, K. Pfingst, and S. D. Peyerimhoff, J. Phys. B **27**, 2297 (1994).

[47] J. Tennyson, J. Phys. B **29**, 6185 (1996).

[48] A. Faure, J. D. Gorfinkiel, L. A. Morgan, and J. Tennyson, Comput. Phys. Commun. **144**, 224 (2002).

[49] T. H. Dunning and P. J. Hay, *Methods of Electronic Structure Theory*, Vol. 2, edited by H. F. Schaefer (Plenum, New York, 1977).

[50] J. Ivanic, G. J. Atchity, and K. Ruedenberg, J. Chem. Phys. **107**, 4307 (1997).

[51] S. Kaur, K. L. Baluja, and J. Tennyson, Phys. Rev. A **77**, 032718 (2008).

[52] S. Kaur and K. L. Baluja, Phys. Rev. A **80**, 042701 (2009).

[53] J. Tennyson and C. J. Noble, Comput. Phys. Commun. **33**, 421 (1984).

[54] Y. K. Kim, W. Hwang, and N. M. Weinberger, M. A. Ali, and M. E. Rudd, J. Chem. Phys. **106**, 1026 (1997).

[55] S. Kaur and K. L. Baluja, Phys. Rev. A **82**, 022717 (2010).

[56] F. A. Gianturco and A. Jain, Phys. Rep. **143**, 347 (1986).

[57] N. Sanna and F. A. Gianturco, Comput. Phys. Commun. **114**, 142 (1998).

[58] P. Baille, J. S. Chang, A. Claude, R. M. Hobson, G. L. Ogram, and A. W. Yau, J. Phys. B **14**, 1485 (1981).